Journal Pre-proofs

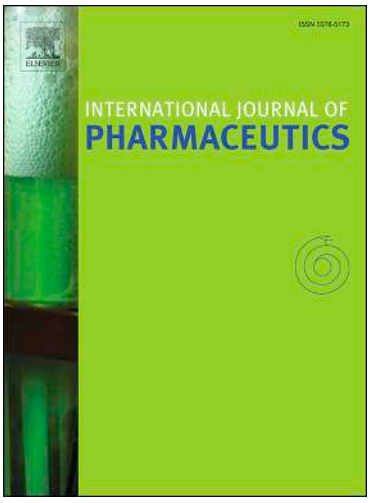

Development of Ferulic Acid/Cyclodextrin Inclusion Complex Nanofibers for Fast-Dissolving Drug Delivery System

Asli Celebioglu, Tamer Uyar

PII: S0378-5173(20)30379-3
DOI: https://doi.org/10.1016/j.ijpharm.2020.119395
Reference: IJP 119395

To appear in: *International Journal of Pharmaceutics*

Received Date: 2 April 2020
Revised Date: 27 April 2020
Accepted Date: 29 April 2020

Please cite this article as: A. Celebioglu, T. Uyar, Development of Ferulic Acid/Cyclodextrin Inclusion Complex Nanofibers for Fast-Dissolving Drug Delivery System, *International Journal of Pharmaceutics* (2020), doi: https://doi.org/10.1016/j.ijpharm.2020.119395

Development of Ferulic Acid/Cyclodextrin Inclusion Complex Nanofibers for Fast-Dissolving Drug Delivery System

Asli Celebioglu* and Tamer Uyar*

Department of Fiber Science & Apparel Design, College of Human Ecology, Cornell University, Ithaca, NY, 14853, United States

*Corresponding Authors: AC: ac2873@cornell.edu; TU: tu46@cornell.edu

ABSTRACT:

Production of electrospun nanofibrous mats of cyclodextrin inclusion complexes with the incorporation of drug molecules would enable promising designing of fast dissolving delivery systems (FDDS) for oral treatments. Here, the single-step electrospinning technique has been applied to prepare cyclodextrin inclusion complex nanofibrous mats (CD-IC NM) of ferulic acid from complete aqueous systems without using any polymeric matrix. The free-standing ferulic acid/CD-IC NM have been electrospun from two different modified cyclodextrin derivatives of hydroxypropyl-beta-cyclodextrin (HP-β-CD) and hydroxypropyl-gamma-cyclodextrin (HP-γ-CD). The initial content of ferulic acid (1/1 ferulic acid/CD (molar ratio) and ~11 % (w/w)) has been protected in case of both ferulic acid/CD-IC NM and so the electrospun nanofibrous mats have been fabricated by the ~100 % loading efficiency. It has been detected from the *in vitro* release and disintegration tests that, the amorphous state of ferulic acid based on inclusion complex formation, and the highly porous feature and high surface area of nanofibrous mats have ensured the fast dissolution/release of ferulic acid and disintegration of nanofibrous mats into the liquid medium and artificial saliva. Herein, HP-γ-CD has formed inclusion complexes with ferulic acid more favorably than HP-β-CD and this has leaded to the existence of some un-complexed ferulic acid crystals in ferulic acid/HP-β-CD-IC NM while, ferulic acid has been completely complexed and is in amorphous state in ferulic acid/HP-γ-CD-IC NM. Furthermore, the thermal stability of ferulic acid has been enhanced as an inclusion complexation aid observed by the shift of thermal degradation temperature of ferulic acid from the range of ~120-200 °C to ~140-280 °C.

KEYWORDS: ferulic acid; cyclodextrin; fast-dissolving delivery system; nanofibers; electrospinning

1. Introduction

In recent decades, fast-dissolving delivery systems (FDDS) has gained great attention in the pharmaceutical industry as a new formulation of treatments (Bala et al., 2013; Kathpalia and Gupte, 2013). Apart from conventional solid dosage form, FDDS can rapidly disintegrate and/or dissolve in the oral cavity upon contact with saliva with neither additional water nor chewing, and they can provide an enhanced solubility, delivery and bioavailability for some of the active pharmaceutical ingredients (APIs) which have trouble of poor water solubility (Bala et al., 2013; Kathpalia and Gupte, 2013). The FDDS can address wide range of patients from children to elderly who have difficulty in swallowing/chewing or suffer from vomiting, nervous/muscular system disorders, allergic attack etc (Bala et al., 2013; Kathpalia and Gupte, 2013; Patel et al., 2011). The FDDS are also useful for the patients who are bedridden; on the decreased liquid-intake plan; travelling (which can restrict the water intake); or having local therapies for toothaches, cold sore, oral ulcers etc (Bala et al., 2013; Kathpalia and Gupte, 2013; Patel et al., 2011). The FDDS are obtainable in various dosage forms; including tablets (Rahane and Rachh, 2018), capsules (Ciper and Bodmeier, 2005), films/strips (Bala et al., 2013; Kathpalia and Gupte, 2013), patches/wafers (Patil et al., 2014). On the other hand, the mouthfeel is an important issue to be concerned for the patient, since the large particles which are slowly disintegrated from the product and slowly dissolved in the saliva would cause some unpleasant feeling during the treatments.

There are several techniques explored and applied in order to formulate the FDDS types such as; solvent casting, tableting, extrusion, spraying, lyophilization (Bala et al., 2013; Ciper and Bodmeier, 2005; Kathpalia and Gupte, 2013; Patel et al., 2011; Patil et al., 2014; Rahane and Rachh, 2018). In recent years, nanotechnological techniques have begun to be investigated as an alternative approach to formulate the FDDS. Electrohydrodynamic atomization (EHDA) technique

of electrospinning is a quite versatile, useful and flexible approach in order to fabricate nano-sized fibrous mats by the incorporation of various active compounds and drug molecules (Seif et al., 2015; Uyar and Kny, 2017; Yu et al., 2018). The electrospun nanofibers are promising candidate as orally FDDS, since the high porosity, large surface area to volume ratio and 3D continuous web structure of nanofibers ensure the fast disintegration and dissolution of these nanofibrous mats upon contact with the liquid medium (Seif et al., 2015; Yu et al., 2018). In addition, these free-standing nanofibrous mats can incorporate the drug molecules in the amorphous state, because the rapid evaporation of solvents inhibits the drug crystallization during the electrospinning process (Seif et al., 2015; Yu et al., 2018). It is obvious that the electrospun FDDS can offer more rapid onset of action and quicker absorption of drugs through the oral cavity compared the conventional dosage form and can avoid the unpleasant grainy feeling during their administration owing to faster dissolution and disintegration profiles of drug incorporated nanofibrous mats.

As an emerging novel dosage form of electrospun FDDS, the water solubility of various biopharmaceutical classification system (BCS) class II-IV drugs was improved by incorporating into hydrophilic polymers via electrospinning (Bukhary et al., 2018; Nam et al., 2017; Sipos et al., 2019; Thakkar et al., 2019; Tort et al., 2019). Polyvinylpyrrolidone (PVP) is one of the most prominent polymer type in order to produce electrospun FDDS and poorly water soluble drugs of aceclofenac (Sipos et al., 2019), ornidazole (Tort et al., 2019), amlodipine besylate/valsartan (Bukhary et al., 2018), paracetamol/caffeine (Illangakoon et al., 2014) incorporated PVP nanofibrous mats have shown fast-dissolving and fast-disintegration behavior. Besides, gelatin (Mano et al., 2017), polyvinyl alcohol (PVA) (Nam et al., 2017), Eudragit (Giram et al., 2018) and polymer blends of chitosan/pullulan (Qin et al., 2019) and PVP/PVA (Thakkar et al., 2019) were also used in order to obtain electrospun FDDS by the incorporation of variety of drug molecules

including phloretin (Nam et al., 2017), moxifloxacin hydrochloride (Giram et al., 2018), aspirin (Qin et al., 2019), repaglinide (Thakkar et al., 2019), etc.

Cyclodextrins (CDs) are a class of oligosaccharides which have an important role in the pharmaceutical research and global market (Bilensoy, 2011; Kalepu and Nekkanti, 2015). The non-covalent host-guest interaction between CD and drug molecules can provide an enhanced stability, apparent solubility and bioavailability for drugs (Bilensoy, 2011; Carneiro et al., 2019; Kalepu and Nekkanti, 2015). Moreover, CD inclusion complexes can mask the unpleasant taste of drugs, inhibit the tissue irritation and ensure a wide range of drug release profile from controlled/sustained to fast (Bilensoy, 2011; Carneiro et al., 2019; Kalepu and Nekkanti, 2015). The solubilizing effect of CD inclusion complexes is especially advantageous in case of insoluble or poorly water-soluble drugs, since it also leads to a significant improvement in bioavailability (Bilensoy, 2011; Carneiro et al., 2019; Kalepu and Nekkanti, 2015; Topuz and Uyar, 2019). Recent studies regarding the electrospinning of nanofibers from the hydrophilic polymers of PVP (Samprasit et al., 2015), PVA (Kazsoki et al., 2018) and gelatin (Aytac et al., 2019) incorporating CD/drug inclusion complexes have been reported for the purpose of fast-dissolving and rapid releasing of drug molecules including meloxicam (Samprasit et al., 2015), metoclopramide (Kazsoki et al., 2018) and ciprofloxacin (Aytac et al., 2019). On the other hand, we have very recently shown the electrospinning of polymer free nanofibers based on the CD inclusion complexes of different drugs (sulfisoxazole (Yildiz et al., 2017), paracetamol (Yıldız and Uyar, 2019), ibuprofen (Celebioglu and Uyar, 2019a), metronidazole (Celebioglu and Uyar, 2019b) and hydrocortisone (Celebioglu and Uyar, 2020)) which can be a promising alternatives of the orally FDDS. The electrospinning of the polymer-free and fast-dissolving nanofibers of CD inclusion complexes with different drugs have been also reported by other research groups (diclofenac

sodium (Balogh et al., 2015) and voriconazole (Vass et al., 2019)). The use of CD as a fiber carrier provides an advantages over polymeric matrix, since CD can form inclusion complexes with drug molecules differently from polymers and that provides simultaneously enhanced solubility and bioavailability of the drugs (Bilensoy, 2011; Carneiro et al., 2019). Moreover, water is the only solvent system in order to form the inclusion complexes and so there is no need to use acid and/or organic solvent to solve the drug molecules in the electrospinning solutions which is quite common and possible in case of polymeric systems.

Ferulic acid (4-hydroxy-3-methoxycinnamic acid) is a natural phenolic acid type which is abundantly found in the plant-based foods including fruits, vegetables and cereals (Zhao and Moghadasian, 2008). Recent studies have shown that ferulic acid displays a wide range of physiological properties such as; antioxidant, anticarcinogen, anti-inflammatory, antimicrobial and neuroprotective (Kumar and Goel, 2019; Mancuso and Santangelo, 2014). Therefore, ferulic acid proposes potential application for pharmaceuticals, food and cosmetic (Kumar and Goel, 2019; Mancuso and Santangelo, 2014). However, the low water solubility and stability of ferulic acid results in lack of bioavailability and activity which limit further applications in concerned areas (Kumar and Goel, 2019; Mancuso and Santangelo, 2014). Several studies have been reported to indicate the enhanced solubility, bioavailability and stability of ferulic acid by the cyclodextrin inclusion complexation (Hsu et al., 2019; Juni Ekowati et al., 2016; Olga et al., 2015; Wang et al., 2011). Even, the encapsulation of ferulic acid within electrospun nanofibers for the purpose of sustained (Poornima and Korrapati, 2017; Xu et al., 2015; Yan et al., 2014; Yang et al., 2017) or fast-release (Huang et al., 2018; Quan et al., 2011; Wang et al., 2017) have been reported. Additionally, the potential of ferulic acid incorporated nanofibrous mats for the treatment of cancer (Balan et al., 2020), tissue engineering (Wang et al., 2013) and antibacterial/antitumor purposes

(Yakub et al., 2018) have been shown within the previous reports. Yet, to the best of our knowledge, there is no report regarding the electrospinning of fast-dissolving electrospun nanofibrous mats of cyclodextrin ferulic acid inclusion complexes. Here, we have developed fast-dissolving oral drug delivery system based on the polymer-free electrospun nanofibrous mats of ferulic acid/cyclodextrin inclusion complexes (ferulic acid/CD-IC NM) using two different hydroxy-propylated derivatives of cyclodextrin (hydroxypropyl-beta-cyclodextrin (HP-β-CD) and hydroxypropyl-gamma-cyclodextrin (HP-γ-CD)) (Fig. 1a). The further analyses have been performed in order to reveal the structural character and release/disintegration profile of samples.

2. Materials and methods

2.1. Materials

Ferulic acid (trans-4-Hydroxy-3-methoxycinnamic acid, 99%, Alfa Aesar), sodium chloride ((NaCl), >99%, Sigma Aldrich), potassium persulfate (($K_2S_2O_8$), 99%, Acros Organics), o-phosphoric acid (85% (HPLC), Fisher Chemical), sodium phosphate dibasic heptahydrate ((Na_2HPO_4), 98.0-102.0%, Fisher Chemical), potassium phosphate monobasic ((KH_2PO_4), ≥99.0%, Fisher Chemical), and deuterated dimethylsulfoxide ((*d6*-DMSO), 99.8%, Cambridge Isotope), were obtained commercially. Hydroxypropyl-beta-Cyclodextrin (HP-β-CD) (Cavasol W7 HP, Mw:1500 g/mol, DS: ~ 0.9,) and Hydroxypropyl-gamma-Cyclodextrin (HP-γ-CD) (Cavasol W8 HP Pharma, Mw:1540 g/mol, DS: ~ 0.6,) were given by Wacker Chemie AG (USA) for scientific researches. All reagents were used without further purification. High quality distilled water was used where required.

2.2. Phase solubility analysis

For phase solubility analysis, we have referred to the method of Higuchi and Connors (Higuchi and Connors, 1965). Here, the excess amount of ferulic acid and modified CD (HP-β-CD and HP-

γ-CD) with concentrations from 0 to 8 mM were mixed in 5 mL of distilled water in glass vials. Then, glass vials were shaken in the dark (450 rpm, 25 ^{o}C) for 24 hours using incubator shaker. After equilibrating, the aqueous systems were filtered through membrane filters (0.45µm, PTFE) in order to remove the undissolved ferulic acid. Each experiment was performed in triplicate and the ultimate filtrates were measured using the UV-Vis spectrophotometry (Lambda 35, PerkinElmer). The intensity of absorbance at 287 nm was taken into consideration for each system and adapted to the concentration (mM) using calibration curve having linearity and acceptability with $R^2 \geq 0.99$. The average spectrophotometric data were used to plot the phase solubility diagrams. The following equations were used to determine the binding constant (K_s) (Higuchi and Connors, 1965) and the complexation efficiency (CE) (Loftsson et al., 2005);

$$K_s = \text{slope}/S_0(1\text{-slope})$$

$$CE = \text{slope}/(1\text{-slope})$$

where S_0 is the intrinsic solubility of ferulic acid in the absence of CD.

2.3. Preparation of electrospun nanofibrous mats

The aqueous systems comprising of ferulic acid/cyclodextrin inclusion complexes (ferulic acid/CD-IC) were used in order to fabricate the ferulic acid/cyclodextrin inclusion complex nanofibrous mats (ferulic acid/CD-IC NM) via electrospinning technique. Initially, the clear CD (hydroxypropyl-beta-cyclodextrin (HP-β-CD) and hydroxypropyl-gamma-cyclodextrin (HP-γ-CD)) solutions were prepared in water with 180% (w/v) solid concentration. Then, ferulic acid was added to each CD (HP-β-CD and HP-γ-CD) solutions to ensure the 1/1 ferulic acid/CD, molar ratio for inclusion complex formation. The aqueous systems were kept constant stirring for 24 hours at ambient conditions. While ferulic acid/HP-γ-CD system became clear, ferulic acid/HP-β-CD systems turned into turbid by the end of stirring. Additionally, the pure aqueous solutions of

HP-β-CD and HP-γ-CD (200%, w/v) were prepared to produce pristine HP-β-CD NM and HP-γ-CD NM. Prior the electrospinning process, the solution properties of viscosity and conductivity, which influence the ultimate fiber morphology, were evaluate, as well. The rheometer (AR 2000 rheometer, TA Instrument) was conducted to determine the viscosity of the CD and ferulic acid/CD-IC solutions (CP 20-4 spindle type (4^{o}), 0.01-1000 s^{-1} (shear rate), 22 ^{o}C), and the conductivity-meter (FiveEasy, Mettler Toledo) was used to measure the conductivity of all solutions.

Here, the electrospinning system (Spingenix, model: SG100, Palo Alto, USA) was used to produce nanofibrous mats. The pure CD and ferulic acid/CD systems were loaded into 1 mL plastic syringe equipped with a 23-gauge stainless steel needle and fixed horizontally on the syringe pump. The constant flow rate of 0.5 mL/h and constant voltage of 15 kV were applied during the electrospinning process. The deposition of as-spun nanofibrous mats were done on the grounded stable metal plate which was located at 15 cm far from the needle and wrapped with a piece of aluminium foil (temperature: ~20 ^{o}C and relative humidity: ~25%).

2.4. Morphology analysis

The morphology of the CD NM (HP-β-CD and HP-γ-CD) and ferulic acid/CD-IC NM was assessed by using scanning electron microscopy (SEM, Tescan-MIRA3). Before the measurements, each sample were Au/Pd sputter-coated under vacuum to eliminate their charging problem. SEM imaging was performed at the excitation voltage of 12 kV and working distance of 10 mm. The average diameter (AD, mean ± standard deviation) of fibers were determined by analyzing more than 100 fibers from the different locations in SEM images using ImageJ software.

2.5. Structural analyses

Proton nuclear magnetic resonance (^{1}H-NMR) measurements were utilized to calculate molar ratio between ferulic acid and CD in ferulic acid/CD NM, and so the loading capacity and loading efficiency of ferulic acid in electrospun mats. All ^{1}H-NMR measurements were carried out on magnetic resonance spectrometer having autosampler (NMR, Bruker AV500) at 25 ^{o}C. ^{1}H-NMR solutions of samples were prepared in *d6*-DMSO at the sample concentration of 40 mg/mL and spectra were recorded by 16 scans. The chemical shifts (δ) were represented in ppm (parts per million) with TSP signal (0 ppm) as the external standard. The^{1}H-NMR data were processed with Mestranova software. For the calculation of the molar ratio, -CH_3 peak of CD at 1.03 ppm and the protons of ferulic acid observed between 6.40-7.60 ppm were considered.

The FTIR spectra of ferulic acid powder, pristine HP-β-CD NM and HP-γ-CD NM, ferulic acid/HP-β-CD-IC NM and ferulic acid/HP-γ-CD-IC NM were obtained by attenuated total reflectance Fourier transform infrared spectrometer (ATR-FTIR, PerkinElmer, USA). The FTIR spectra in absorption mode were obtained at the region of 4000 and 600 cm^{-1} and the resolution of 4 cm^{-1} upon 64 scans.

The X-ray diffraction patterns of ferulic acid powder, pristine HP-β-CD NM and HP-γ-CD NM, ferulic acid/HP-β-CD-IC NM and ferulic acid/HP-γ-CD-IC NM were determined by X-ray diffractometer (Bruker D8 Advance ECO) and Cu Kα radiation. The XRD scans were carried out in the 2Θ range of 5^o-30^o under the 40 kV and 25 mA operating parameters.

Thermal properties of ferulic acid powder, pristine HP-β-CD NM and HP-γ-CD NM, ferulic acid/HP-β-CD-IC NM and ferulic acid/HP-γ-CD-IC NM were examined by differential scanning calorimeter (DSC, Q2000, TA Instruments, USA) and thermogravimetric analyzer (TGA, Q500, TA Instruments, USA). The DSC measurements were conducted from 0 ^{o}C to 210 ^{o}C at a heating rate of 10 ^{o}C/min. For TGA analyses, each sample was heated from 30 ^{o}C to 550

°C at 20 °C/min heating rate. For both thermal analyses of DSC and TGA, N_2 gas was used in order to ensure the inert atmosphere.

2.6. In vitro release test

The in vitro release profiles of ferulic acid/HP-β-CD-IC NM and ferulic acid/HP-γ-CD-IC NM were examined by the dissolution of same amount of sample (~ 40 mg) in 40 mL of distilled water. The profiles of nanofibrous mats were compared with the powder of ferulic acid, as well. For this, ~ 4.5 mg ferulic acid powder was used which corresponds to the initial ferulic acid content in ferulic acid/CD-IC NM. Here, ferulic acid/CD-IC NM and ferulic acid powder were placed in beaker, separately than distilled water was poured into each sample. All systems were shaken on the incubator with the speed of 200 rpm at room temperature. For the analyses, 500 µL of the dissolution liquid was withdrawn and 500 µL of fresh distilled water was refilled at the pre-determined time points. The withdrawn samples were analyzed using UV-Vis spectroscopy to quantify the dissolved ferulic acids in the medium. The maximum absorbance of ferulic acid at 287 nm was considered for the calculations and the measurements results were adapted to the concentration (µg/mL) by the calibration curve having linearity and acceptability with $R^2 \geq 0.99$. To investigate the kinetic behavior of samples, different mathematical models were applied including; zero and first-order release model, Higuchi release model and Korsmeyer-Peppas equation (see supporting information) (Peppas and Narasimhan, 2014).

2.7. Disintegration behavior

The disintegration profiles of pristine CD NM and ferulic acid/CD-IC NM were evaluated using a technique which was developed by Bi et al. to simulate the physiological conditions of a moist tongue (Bi et al., 1996). For the test, we have slightly modified the technique and firstly a piece of water-absorbable sponge was placed in a petri dish (diameter; 3.5 cm). Then, these sponges were

thoroughly wetted with artificial saliva (10 mL). Here, the artificial saliva was prepared by dissolving 1.19 g Na_2HPO_4, 95 mg KH_2PO_4 and 4 g NaCl in 500 mL of distilled water and arranging the pH of the system as 6.8 with phosphoric acid. After the sponges were wetted properly, the excess artificial saliva was drained out from the petri dishes and a piece of nanofibrous mat (~ 14 mg) was placed on the sponge at room temperature. The disintegration profile of nanofibrous mats was recorded as video.

2.8. Statistical analysis

The results of the replicated experiments ($n \geq 3$) were given as mean values ± standard deviations. The one-way or two-way of variance (ANOVA) were applied for the statistical analyses. The OriginLab (Origin 2019, USA) was used for the ANOVA analyses (0.05 level of probability).

3. Results and discussions

3.1. Phase solubility analysis

In this study, the phase solubility technique described by Higuchi and Connors was carried out in order to examine the effect of HP-β-CD and HP-γ-CD on the solubilization of ferulic acid (Higuchi and Connors, 1965). The stability constant (Ks) and the complexation efficiency (CE) were also determined using phase solubility diagram to evaluate the physicochemical properties of ferulic acid in the presence of CD molecules (Higuchi and Connors, 1965; Loftsson et al., 2005; Saokham et al., 2018). Fig. 2 shows the phase solubility diagrams of ferulic acid/HP-β-CD and ferulic acid/HP-γ-CD systems. The solubility manner of ferulic acid was tested against the increasing concentration of CD from 0 to 8 mM. For both modified CD types, the increment in ferulic acid solubility was observed as a linear function of CD concentration which is classified as a A_L-typed profile (Higuchi and Connors, 1965). According to Higuchi and Connors, the linear relationship

suggested the formation of inclusion complexes between ferulic acid and CD with the 1:1 molar stoichiometry (Higuchi and Connors, 1965; Saokham et al., 2018). This finding are also coherent with the previous studies in which the phase solubility profile of ferulic acid and modified CD were obtained with a typical A_L profile (Mori et al., 2019; Wang et al., 2011). Due to the inclusion complexation, the 8 mM concentrated solutions of HP-β-CD and HP-γ-CD could dissolve 2.6- and 3.5-fold higher amount of ferulic acid, respectively compared to the solution without CD. As shown in Fig. 2, the stability constants (K_s) of ferulic acid/HP-β-CD and ferulic acid/HP-γ-CD systems were determined to be 468 M^{-1} and 2490 M^{-1}, respectively which propose the stable complexation between ferulic acid and CD, and this is crucial for improving the limited bioavailability of this active compound (Hsu et al., 2019). The statistical analysis also demonstrated the significant difference between ferulic acid/HP-β-CD and ferulic acid/HP-γ-CD systems by the p value which is less than 0.05. These results suggested that, the ferulic acid forms more favorable and stable inclusion complexes with HP-γ-CD compared to HP-β-CD, and so HP-γ-CD ensures better water solubility for ferulic acid. The reason might be the better size match and thermodynamic interactions between ferulic acid and HP-γ-CD compared to HP-β-CD which lead to higher K_s value along with solubilizing effect for ferulic acid/HP-γ-CD system (Saokham et al., 2018). In other related studies, the stability constants were released with the different values of 166.3 M^{-1} (Wang et al., 2011) and 218.5 M^{-1} (Mori et al., 2019) for ferulic acid/HP-β-CD system and 477.5 M^{-1} (Mori et al., 2019) for ferulic acid/HP-γ-CD system. Although, the stability constant values are not the same with the literature, the higher K_s value and solubilizing effect of ferulic acid/HP-γ-CD system are in the line with the previous study reported by Mori et al. In the given study, HP-γ-CD provided higher solubility enhancement and so stability constant for ferulic acid molecules among other CD types (Mori et al., 2019). As mentioned in one of the previous study,

the K_s value of the same guest/CD system might be triggered because of the difference of the substitution degree of the HP groups in hydroxy-propylated CD derivatives (Loftsson et al., 1994). The substitution degree of the HP-β-CD and HP-γ-CD were not mentioned in the previous studies (Mori et al., 2019; Wang et al., 2011), however we have obtained the stability constant of 468 M^{-1} and 2490 M^{-1} for HP-β-CD and HP-γ-CD systems having substitution degree of ~ 0.9 and ~ 0.6, respectively. It is worth noting that, another reason for the more favorable complex formation between ferulic acid and HP-γ-CD compared to HP-β-CD might be the lower substitution degree of HP-γ-CD. Since, the increasing substitution degree of the CD derivatives can inhibit the accessibility of CD cavity and can reduce the binding strength between CD and guest compound (Loftsson et al., 1994). The phase solubility diagram has also enabled to calculate the CE value for both systems of HP-β-CD and HP-γ-CD. The CE values were determined as 1.3 and 7.0 for HP-β-CD and HP-γ-CD systems, respectively. According to Loftsson et al. (Loftsson et al., 2005), CE value of 1.3 implies that 1 out of every 1.75 HP-β-CD molecules in the solution tend to form soluble complexes with the ferulic acid molecules. On the other hand, CE value of 7.0 means that 1 out of every 1.15 HP-γ-CD molecules can form complexes with the ferulic acid molecules. As is seen, CE value also demonstrated that the higher ratio of HP-γ-CD molecules intended to join complexation process compared to HP-β-CD molecules under the conducted experimental conditions.

3.2. Morphology of nanofibrous mats

As it has been reported previously, ferulic acid favorably form 1/1 (ferulic acid/CD) inclusion complexes with the hydroxy-propylated derivatives of CD molecules (Hsu et al., 2019; Juni Ekowati et al., 2016; Mori et al., 2019; Olga et al., 2015; Wang et al., 2011). Therefore, we have prepared ferulic acid/HP-β-CD and ferulic acid/HP-γ-CD aqueous systems having 1/1 molar ratio.

The concentration of both HP-β-CD and HP-γ-CD were set to 180 % (w/v) for the electrospinning of ferulic acid/CD inclusion complex (IC) nanofibrous mats (NM). As control sample, the aqueous solutions of pure HP-β-CD (200 %, w/v) and HP-γ-CD (200 %, w/v) were prepared, as well in order to produce the pristine HP-β-CD NM and HP-γ-CD NM. While, pure HP-β-CD solution is clear, ferulic acid/HP-β-CD resulted in turbid because of the un-complexed/undissolved ferulic acid (Fig. 3a,b). On the other hand, ferulic acid/HP-γ-CD-IC solutions is clear just like pure HP-γ-CD one, since ferulic acid are fully encapsulated in CD cavity and became water soluble (Fig. 3c,d). It is worth to mention that, the addition of ferulic acid to the CD solution system did not show any negative influence on the electrospinning process. Therefore, all aqueous systems of CD and ferulic acid/CD-IC resulted in self-standing and handy nanofibrous mats which can be folded without any structural damage, demonstrating its suitability for fast dissolving oral delivery systems (Fig. 3). The morphology of pristine CD NM and ferulic acid/CD-IC NM was examined using scanning electronic microscopy (SEM). Fig. 3 shows the representative SEM images of the pristine CD NM and ferulic acid/CD-IC NM. Each nanofibrous mats were successfully produced having uniform and without beads-on-string morphology. Even the ferulic acid/HP-β-CD-IC solutions contained some un-complexed ferulic acid parts (Fig. 3b-i), SEM image did not indicate any crystal structure (Fig. 3b-iii) suggesting the homogenously distributed and small sized crystals of ferulic acid within the fiber mats. Table 1 summarizes the solution properties (viscosity and conductivity) and the average diameter (AD) of fibers for each CD NM and ferulic acid/CD-IC NM. For both CD type, the viscosity of ferulic acid/CD-IC solutions is lower than pure CD solutions, since higher concentration (200%, w/v) was used for the electrospinning of pristine CD NM compared to ferulic acid/CD-IC systems (180%, w/v). On the other hand, the incorporation of ferulic acid led to increase in the conductivity of both of HP-β-CD and HP-γ-CD systems (Table

1). All these variations in the viscosity and conductivity induce differences in the AD values of fibers (Uyar and Besenbacher, 2008; Xue et al., 2019). It is well-known that the lower viscosity and higher conductivity of electrospinning solutions conduce to thinner fiber formation owing to more stretching of the jet in the course of process (Uyar and Besenbacher, 2008; Xue et al., 2019). Thus, electrospinning of pure HP-β-CD resulted in nanofibrous mats having AD of 505±160 nm, whereas the ferulic acid/HP-β-CD-IC NM was obtained having AD of 220±70 nm, since ferulic acid/HP-β-CD-IC solution has higher conductivity and lower viscosity compared to HP-β-CD solutions. The similar trend is also detected in case of HP-γ-CD based systems such that HP-γ-CD NM has AD of 1660±275 nm whereas ferulic acid/HP-γ-CD-IC NM has AD of 1355±505 nm (Table 1). It is also obvious that, the HP-γ-CD based samples (HP-γ-CD NM and ferulic acid/HP-γ-CD-IC NM) have much higher AD values compared to HP-β-CD based samples (HP-β-CD NM and ferulic acid/HP-β-CD-IC NM) (Table 1). Since the lower conductivity and higher viscosity value ranges of HP-γ-CD based solutions led to less stretching of the jet during the fiber formation. The statistical analysis supported the experimental results in which the significant variations were observed between samples ($p < 0.05$).

3.3. Structural characterization

Nuclear magnetic resonance (NMR) spectroscopy is a convenient tool to provide quantitative information about the CD inclusion complexes by calculating the molar ratio between guest and CD molecules (Celebioglu and Uyar, 2019b, 2019a, 2019c). In this study, ^{1}H-NMR measurements were carried out to attain the molar ratio between ferulic acid and CD molecules in ferulic acid/HP-β-CD-IC NM and ferulic acid/HP-γ-CD-IC NM and to determine the loading capacity and loading efficiency of the ferulic acid/CD-IC NM samples. The initial molar ratio:1/1 (ferulic acid/CD) was used for the preparation of ferulic acid/CD aqueous systems which corresponds to the ~11 % (w/w)

of ferulic acid content in electrospun ferulic acid/CD-IC NM. However, the ultimate nanofibrous mats might contain lower amount of ferulic acid than their initial state, because of a potential loss through the preparation step or electrospinning process. Fig. 4 indicates the ^{1}H-NMR spectra of pure ferulic acid, ferulic acid/HP-β-CD-IC NM and ferulic acid/HP-γ-CD-IC NM. For the calculation of the molar ratio between ferulic acid and CD, the integration of the -CH_3 peak of CD (HP-β-CD and HP-γ-CD) at 1.03 ppm and the protons of ferulic acid assigned between 6.40-7.60 ppm (Hsu et al., 2019) were proportioned to each other (Fig. 4). In order to obtain a high yield loading efficiency, it is essential to maintain the active compound content at the initial level after all these preparation and electrospinning steps. Fortunately, the ^{1}H-NMR results indicated that the molar ratio of ferulic acid/CD in ferulic acid/HP-β-CD-IC NM and ferulic acid/HP-γ-CD-IC NM was same as the initial level of 1/1. The ^{1}H-NMR data demonstrated that the ferulic acid molecules were efficiently loaded and totally preserved in the ferulic acid/CD-IC NM without any loss of ferulic acid. As it was mentioned in the previous section, there is un-complexed ferulic acid in ferulic acid/HP-β-CD-IC NM. However, the NMR solvent of *d6*-DMSO enabled to dissolve the un-complexed ferulic acid parts in ferulic acid/CD-IC NM, as well and that's why the molar ratio of 1/1 was calculated from ^{1}H-NMR spectrum of ferulic acid/HP-β-CD-IC NM. Briefly, ferulic acid/HP-β-CD-IC NM and ferulic acid/HP-γ-CD-IC NM were successfully fabricated by the loading capacity of ~11 % (w/w) and the loading efficiency of ~ 100 %.

Fourier transform infrared (FTIR) spectroscopy is a useful tool in order to confirm the formation of inclusion complexes between guest and CD molecules (Narayanan et al., 2017). Fig. 5 depicts the FTIR spectra of ferulic acid powder, pristine CD NM and ferulic acid/CD-IC NM recorded in the spectral region of 4000-600 cm^{-1}. The FTIR spectrum of ferulic acid exhibits distinctive absorption bands at 3432 cm^{-1} (-OH stretching); 1688 cm^{-1}, 1661 cm^{-1} (C=O stretching

vibration); 1618 cm^{-1}, 1589 cm^{-1}, 1509 cm^{-1}, 1430 cm^{-1}, 1204 cm^{-1} (aromatic nucleus); 1465 cm^{-1} (C–H deformations and aromatic ring vibrations); 1264 cm^{-1} (C–O–C asymmetric stretching vibration); 1157 cm^{-1} (carbonyl group) and 851 cm-1, 801 cm^{-1} (two adjacent hydrogen atoms on the phenyl ring) (Olga et al., 2015; Wang et al., 2011). In case of HP-β-CD and HP-γ-CD, there are prominent peaks located at around 3324-3355 cm^{-1}, 2930 cm^{-1}, 1650 cm^{-1} and 1370 cm^{-1} corresponds to the vibrations of -OH stretching, C-H stretching, O-H bending and $-CH_3$ bending of CD, respectively. The other major absorption bands observed at 1028 cm^{-1}, 1150 cm^{-1} and 1180 cm^{-1} correspond to vibrations of coupled C–C/C–O stretching and antisymmetric C–O–C glycosidic bridge stretching of CD (Olga et al., 2015; Wang et al., 2011; Yuan et al., 2015). It is observed that the full range FTIR spectra of ferulic acid/CD-IC NM are very similar to pristine CD NM spectra and the absorption bands of ferulic acid are almost hidden by the broad and intense bands of CD in case of ferulic acid/CD-IC NM, substantially due to higher content of CD (~ 89%, w/w) in the samples. On the other hand, the expanded FTIR spectra of samples indicated that, several ferulic acid peaks are obvious in the ferulic acid/CD-IC NM spectra with attenuated and shifted profile differently from pure ferulic acid spectrum (Fig. 5-i,ii,iii). It is quite well-known that, the attenuation/disappearance, shifts and/or broadening of the characteristic peaks of guest molecules in FTIR spectra suggest the interaction between CD and guest molecules by inclusion complexation (Mura, 2015; Narayanan et al., 2017). Here, we have detected that the characteristic peaks of ferulic acid at 1618 cm^{-1}, 1589 cm^{-1}, 1509 cm^{-1}, 1430 cm^{-1}, 1264 cm^{-1}, 851 cm^{-1} and 801 cm^{-1} shifted to 1632 cm^{-1}, 1595 cm^{-1}, 1516 cm^{-1}, 1428 cm^{-1} and 1271 cm^{-1}, 845 cm^{-1} and 816 cm^{-1}, respectively (Fig. 5ii,iii). Additionally, the broad band of ferulic acid located at 1688 cm^{-1}-1661 cm^{-1} converted to an apparent single peak at 1685 cm^{-1} (Fig. 5ii) and the broad peak of CD around 3324-3355 cm^{-1} was decreased in intensity for both ferulic acid/HP-β-CD-IC NM and ferulic

acid/HP-γ-CD-IC NM (Fig. 5i) (Olga et al., 2015; Wang et al., 2011). These observations proved the inclusion complex formation between ferulic acid and CD in ferulic acid/CD-IC NM and all these spectral changes might also suggest that the phenyl ring of ferulic acid was involved in the CD cavity during the inclusion complexation (Fig. 1c). Our findings are supported by the previous reports in which the inclusion complexation mechanism of ferulic acid and CD molecules was evaluated using different kinds of CD and their derivatives (Hsu et al., 2019; Olga et al., 2015; Wang et al., 2011; Zhang et al., 2009). In these studies, it is concluded that the ferulic acid molecules can be encapsulated inside the CD cavity through its hydrophobic part corresponding to the benzene ring with the ethylene moiety and the most polar groups of ferulic acid are close to wider rim of the CD and/or exposed to outside the CD cavity (Fig. 1c) (Hsu et al., 2019; Olga et al., 2015; Wang et al., 2011; Zhang et al., 2009).

The amorphous state and the homogenous distribution of drug molecules within in the nanofibers plays an important role for the fast-dissolution property; along with porous characteristic and large surface area of nanofibrous mats (Yu et al., 2018). X-ray diffractometer (XRD) is a handy tool to examine the crystalline/amorphous state of drug molecules in the nanofibrous mats (Nagy et al., 2015). In the event of inclusion complex formation, guest molecules are encapsulated in CD cavity, separated from each other cannot form crystal aggregates. Since the inclusion complex formation induce differentiation of crystalline state of guest molecules, XRD is also a valuable technique in order to check the inclusion complex formation between guest and CD molecules (Mura, 2015; Narayanan et al., 2017). Fig. 6a showed the XRD patterns of ferulic acid powder, pristine CD NM and ferulic acid/CD-IC NM. The intense and sharp diffraction peaks at 9.1°, 12.8° and 15.6° were detected for ferulic acid powder indicating its crystalline structure. On the other hand, pristine HP-β-CD NM and HP-γ-CD NM displayed broad halo pattern

confirming their amorphous nature. As it was mentioned in the previous section, the solution of ferulic acid/HP-β-CD-IC was turbid indicating the existence of some un-complexed ferulic acid parts (Fig. 2). The XRD finding correlated with the visual examination, and the XRD graph of ferulic acid/HP-β-CD-IC NM has shown very low intensity of ferulic acid crystals demonstrating the few amounts of un-complexed ferulic acid content in the sample (Fig. 6a). In contrast, the ferulic acid/HP-γ-CD-IC NM has shown a broad halo pattern just like pristine HP-γ-CD NM indicating the complete inclusion complexation and amorphization of ferulic acid in case of ferulic acid/HP-γ-CD-IC NM (Fig. 6a) (Juni Ekowati et al., 2016). This result is also correlate with the visual observation where the ferulic acid/HP-γ-CD-IC solution was clear without displaying any hint of un-complexed ferulic acid (Fig. 2).

DSC is a useful analytical tool in order to examine the inclusion complex formation between CD and guest molecules, especially in company with a complementary technique of XRD (Mura, 2015; Narayanan et al., 2017). For instance, the melting or sublimation temperature of guest molecules can disappear in the case of inclusion complexation, or these thermal transitions can be detected in DSC thermograms if un-complexed guest molecules does exist in the sample (Celebioglu et al., 2016; Mura, 2015; Narayanan et al., 2017). Fig. 6b depicts the DSC thermograms of ferulic acid powder, pristine CD NM and ferulic acid/CD-IC NM. DSC curve of ferulic acid displays a sharp endothermic peak at 173 ºC corresponding to its melting point of crystalline state (Fig. 6b) (Olga et al., 2015; Sharif et al., 2018). In case of amorphous pristine CD NM, a broad endothermic band was observed between 30-145 °C corresponding to the release of water from CD cavity (Celebioglu et al., 2016; Sharif et al., 2018). The DSC measurements indicated that the thermograms of ferulic acid/CD-IC NM are very similar to DSC profile of pristine CD NM, along with the broad endothermic peak in the range of 30-145 °C due to the CD

dehydration. However, the DSC thermogram of ferulic acid/HP-β-CD-IC NM has shown a small broadened and shifted endothermic peak having peak area of ~2.0 J/g which confirmed that there are some un-complexed ferulic acid crystals present in the sample (Mura, 2015). In case of ferulic acid/HP-γ-CD-IC NM, no melting point was noticed for ferulic acid revealing that the ferulic acid was completely in inclusion complex state in the nanofibrous matrix (Olga et al., 2015; Rezaei et al., 2019; Sharif et al., 2018). In brief, the DSC results correlate with the visual observations (Fig. 2) and XRD findings (Fig. 6a) proving that the ferulic acid is fully amorphous in ferulic acid/HP-γ-CD-IC NM and there are very small amounts of un-complexed ferulic acid in ferulic acid/HP-β-CD-IC NM. In addition to all these findings, the differences of the total enthalpy change (ΔH in J/g) of dehydration between pristine CD NM and ferulic acid/CD-IC NM can reveal the inclusion complex formation (Celebioglu et al., 2016; Mura, 2015). In case of complexation, guest molecules are replaced with the water molecules locating in the CD cavity. Therefore, ΔH of the dehydration of CD-IC is supposed to be lower compared to pristine CD molecules. Here, dehydration ΔH (J/g) values of the HP-β-CD NM, HP-γ-CD NM, ferulic acid/HP-β-CD-IC NM and ferulic acid/HP-γ-CD-IC NM were determined as 265 J/g, 318 J/g, 153 J/g and 193 J/g, respectively. As is seen, there is a distinct decrease of the ΔH value in case of ferulic acid/CD-IC NM which further supported that the ferulic acid molecules were successfully encapsulated into CD cavity upon inclusion complexation.

The thermal properties of ferulic acid/CD-IC NM was further examined using thermal gravimetric analyzer (TGA). The TGA thermograms and the derivatives of the TG functions of ferulic acid, pristine CD NM and ferulic acid/CD-IC NM were depicted in Fig. 7. The ferulic acid powder has shown two steps of degradation corresponding to the formation of 4-vinylguaiacol (123-207 °C) and the formation of 4-methyl-, and 4-ethylguaiacols (253-395°C) (Sharif et al.,

2018). For pristine HP-β-CD NM and HP-γ-CD NM, dehydration and degradation are two main processes during the heating. The degradation of HP-β-CD NM and HP-γ-CD NM arises between 280-430 °C and 265-420 °C, respectively along with a weight loss at 30-100 °C resulted from dehydration of samples. Different TGA pattern was observed for ferulic acid/HP-β-CD-IC NM and ferulic acid/HP-γ-CD-IC NM; there are three main steps of weight loss which corresponds to the dehydration, thermal degradation of ferulic acid and CD, respectively. Owing to the evaporation of water, the ferulic acid/CD-IC NM have indicated weight loss step below 100 °C just as is seen in pristine CD NM. The degradation of ferulic acid in ferulic acid/CD-IC NM occurred between 146-280 °C and 142-279 °C for ferulic acid/HP-β-CD-IC NM and ferulic acid/HP-γ-CD-IC NM, respectively. The major weight loss possessed at the temperatures ranging from 280 °C to 428 °C and from 279 °C to 425 °C for ferulic acid/HP-β-CD-IC NM and ferulic acid/HP-γ-CD-IC NM, respectively attributed to the thermal degradation of CD in the samples. As is seen in derivative curves, there is no significant change of the thermal degradation range of CD in case of ferulic acid/CD-IC NM compared to pristine ones. However, the weight loss caused by these degradations was reduced in % compared with the pristine CD NM indicating the conjugation of ferulic acid and CD in samples. Furthermore, the first and the main degradation step of ferulic acid (123-207 °C) has shifted to higher temperature ranges (146-280 °C and 142-279 °C) in case of both ferulic acid/CD-IC NM confirming the inclusion complex formation between ferulic acid and CD. The thermal stability improvement for the guest molecule is usually experienced in case of CD inclusion complexes (Narayanan et al., 2017). Recent observations suggested that the encapsulation of ferulic acid into CD molecules can enhance the thermal stability of this active compound and effectively stabilize it by increasing the thermal degradation temperature. Since the second and minor thermal degradation step of ferulic acid was hindered by

the main degradation of CD, the absolute content (%) of ferulic acid in ferulic acid/CD-IC NM could not be calculated from TGA thermograms. On the other hand, the first and the main weight loss belonging the major degradation of ferulic acid was calculated as ~ 9 % (w/w) (146-280 °C) and ~ 8 % (w/w) (142-279 °C) for ferulic acid/HP-β-CD-IC NM and ferulic acid/HP-γ-CD-IC NM, respectively. These results are slightly different from the ^{1}H-NMR findings in which the ferulic acid content in electrospun ferulic acid/CD-IC NM was determined as ~11 % (w/w).

3.4. In vitro release profile

The release of ferulic acid from ferulic acid/HP-β-CD-IC NM and ferulic acid/HP-γ-CD-IC NM were examined and the obtained release profiles are shown in Fig. 8. A remarkable improvement of dissolution and release of ferulic acid in the nanofibrous mats were observed compared to pure ferulic acid (Fig. 8). The ferulic acid/CD-IC NM dissolved immediately upon the contact with dissolution medium and both ferulic acid/CD-IC NM provided similar cumulative release profiles. Ferulic acid/HP-β-CD-IC NM and ferulic acid/HP-γ-CD-IC NM released 107.1±3.5 μg/mL and 108.5±1.9 μg/mL of ferulic acid in the first minute, respectively and the release of ferulic acid showed steady state up to 10 minutes for both samples. On the contrary, pure ferulic acid was freed into the water with a smaller concentration of 17.5±3.8 μg/mL in the first 60 seconds and it reached up to concentration of 42.2±2.3 μg/mL by the end of same period of time (10 minutes). These findings confirm that the inclusion complex state exist in ferulic acid/CD-IC NM provide significant enhancement of fast-dissolution profile of ferulic acid compared to its pure state. The electrospun inclusion complex nanofibrous mats have essential properties for enhancing the dissolution and release of hydrophobic/poorly soluble active compounds (Celebioglu and Uyar, 2020, 2019a, 2019c, 2019b). Here, the improved fast dissolution profile of ferulic acid in ferulic acid/CD-IC NM can be ascribed to the following unique properties of the system: (1) amorphous

distribution of ferulic acid in the nanofibrous matrix due to the inclusion complex formation; (2) the high water solubility of modified cyclodextrins used as electrospinning matrix (HP-β-CD and HP-γ-CD) that promotes the rapid dissolution/disintegration of nanofibrous matrix; (3) the high surface area, porous and the 3D continuous structure of nanofibrous mats which increase the number of contact sides and the penetration ways for the dissolution medium. As it is depicted in Fig. 8, ferulic acid/HP-β-CD-IC NM and ferulic acid/HP-γ-CD-IC NM showed similar released profile for the same sample amount (~ 40 mg) of mats. Once the released concentration of ferulic acid was compared with the theoretical concentration, it was observed that the ~ 96 % and ~ 100 % of ferulic acid was released from ferulic acid/HP-β-CD-IC NM and ferulic acid/HP-γ-CD-IC NM, respectively. As is seen, the ferulic acid/HP-β-CD-IC NM showed lower release % compared to ferulic acid/HP-γ-CD-IC NM because of the some un-complexed ferulic acid in the sample which could not be dissolved in the aqueous medium in the given time of period. It is worth to mentioned that, the statistical analyses indicated that there are significant variations between samples ($p < 0.05$). The release profiles of samples were also examined by fitting to different kinetic models and the correlation coefficient (R^2) values were summarized in Table S1. The R^2 values indicated that, the release profiles of ferulic acid/CD-IC NM are not compatible with neither zero/first order kinetics nor Higuchi model. As Peppas et al. revealed in their study, this finding suggested that the release of ferulic acid is not time dependent and does not occur from a planar matrix which does not dissolve in water (Fick`s first law) (Peppas and Narasimhan, 2014). Among the other models, the release profiles showed the higher coherence with Korsmeyer–Peppas model and the slope of the fitted graphs enabled to determine the diffusion exponent (*n*) value (Table S1). The *n* values for all sample were found $0.45<n<0.89$ range indicating the irregular or non-Fickian diffusion referring to the combination of diffusion and erosion-controlled release of ferulic acid

(Li et al., 2013; Peppas and Narasimhan, 2014). In one of the related study of Li et at., the *n* value was also determined between the same range (0.6242 and 0.7904) for caffeine and riboflavin incorporated poly(vinyl alcohol) (PVA) nanofibers indicating fast-dissolving profile due to the hydrophilic nature of PVA polymer (Li et al., 2013). Briefly, the collective synergistic action of nanosized fiber structure and the molecular encapsulation of ferulic acid in the cyclodextrin fiber matrix provided an enhanced dissolution rate and so release of ferulic acid which suggested that the ferulic acid/CD-IC NM might be utilized as fast-dissolving oral delivery system.

3.5. Disintegration profile

The disintegration tests were performed using the sponge material which was wetted with artificial saliva and considered as a simulant of moist tongue (Bi et al., 1996; Kwak et al., 2017). Fig. 9 and Movie S1 indicated the disintegration process of pristine CD NM and ferulic acid/CD-IC NM. Here, the ferulic acid/CD-IC NM behaves in the same way with pristine nanofibrous mats and all sample immediately absorbed artificial saliva from the wet sponge and so disintegrated by the contact (Fig. 9). Since the sponge surface is rough, there are barely un-contacted and so un-disintegrated parts of samples as observed at the ≤ 2s, but these parts also disappeared instantly as shown in Fig. 9. Here also, the high-water solubility of modified CD (HP-β-CD and HP-γ-CD), inclusion complexation, high surface area to volume ratio and porosity of nanofibrous mats are the key dynamics for the fast disintegration profile of nanofibrous mats as in fast dissolution profile (Kwak et al., 2017). The fast dissolution and disintegration are crucial factors for fast-dissolving delivery systems, since it provides an immediate treatment in case of need and eliminates the challenges for the patients who suffer from swallowing and absorbing water (Almukainzi et al., 2019; Bala et al., 2013; Kathpalia and Gupte, 2013). Therefore, the disintegrating property in a little amount of saliva can be vital during these types of treatments (Almukainzi et al., 2019; Bala

et al., 2013; Kathpalia and Gupte, 2013). To conclude, ferulic acid/CD-IC NM can be considered as a promising formulation for the fast-dissolving delivery systems by the easy penetration of saliva and enhancing the water solubility of ferulic acid by inclusion complexation.

4. Conclusion

Cyclodextrins draw great attention for use in drug formulations since they provide non-negligible enhancement for the water solubility, bioavailability and stability of poorly water-soluble drug molecules by forming inclusion complexes. On the other hand, the electrospun nanofibers, generated on a large scale, also attracts attention in both scientific studies and industrial applications. In particular, the amorphous composites of nanofiber and drugs hold promises for the developing of fast dissolving delivery systems. In the current report, the polymer-free inclusion complex nanofibrous mats of ferulic acid and cyclodextrins were fabricated using the two derivatives of hydroxypropyl-beta-cyclodextrin (HP-β-CD) and hydroxypropyl-gamma-cyclodextrin (HP-γ-CD) which have high water solubility. The free-standing, defect-free and homogenous nanofibrous mats were obtained for both CD types with the loading efficiency of ~100%. By inclusion complexation, the amorphous distribution of ferulic acid has been ensured through the nanofibrous mat and both HP-β-CD and HP-γ-CD effectively have enhanced the water-solubility of ferulic acid. Here, HP-γ-CD has depicted higher solubilizing improvement for ferulic acid compared to HP-β-CD. In addition to fast-dissolution and so the immediate release of ferulic acid from electrospun nanofibrous mats, ferulic acid/CD-IC NM have also disintegrated instantly when contact to artificial saliva. It is worthy of note that, water is the only solvent type using in the electrospinning of ferulic acid/CD-IC NM and this is a great advantage for the commercialization of cyclodextrin inclusion complex nanofibrous mats. We anticipate that ferulic acid/CD-IC NM can potentially pave the way of the development for new generation fast-

dissolving oral drug delivery system due to the various advantage coming from both cyclodextrin and electrospinning technique.

CRediT authorship contribution statement

Asli Celebioglu: Conseptualization, Methodology, Validation, Investigation, Writing-Original draft preparation, Writing-Review & Editing. **Tamer Uyar:** Supervision, Resources, Conseptualization, Methodology, Project administration, Funding acquisition.

Declaration of Competing Interest

The Authors declare that they have no known competing financial interests or personal relationships that could have appeared to influence the work reported in this paper.

Acknowledgments

This work made use of the Cornell Center for Materials Research Shared Facilities which are supported through the NSF MRSEC program (DMR-1719875), and the Cornell Chemistry NMR Facility supported in part by the NSF MRI program (CHE-1531632), and the Department of Fiber Science & Apparel Design facilities. Prof. Uyar acknowledges the startup funding from the College of Human Ecology at Cornell University. The partial funding for this research was also graciously provided by Nixon Family (Lea and John Nixon) thru College of Human Ecology at Cornell University.

Disclosure

The authors report no conflicts of interest in this work.

Appendix A. Supplementary data

Supplementary data to this article can be found online at https:// doi.org/XXX

References

Almukainzi, M., Araujo, G.L.B., Löbenberg, R., 2019. Orally disintegrating dosage forms. J. Pharm. Investig. 49, 229–243.

Aytac, Z., Ipek, S., Erol, I., Durgun, E., Uyar, T., 2019. Fast-dissolving electrospun gelatin nanofibers encapsulating ciprofloxacin/cyclodextrin inclusion complex. Colloids Surfaces B Biointerfaces 178, 129–136.

Bala, R., Khanna, S., Pawar, P., Arora, S., 2013. Orally dissolving strips: A new approach to oral drug delivery system. Int. J. Pharm. Investig. https://doi.org/10.4103/2230-973x.114897

Balan, P., Indrakumar, J., Murali, P., Korrapati, P.S., 2020. Bi-faceted delivery of phytochemicals through chitosan nanoparticles impregnated nanofibers for cancer therapeutics. Int. J. Biol. Macromol. 142, 201–211.

Balogh, A., Horváthová, T., Fülöp, Z., Loftsson, T., Harasztos, A.H., Marosi, G., Nagy, Z.K., 2015. Electroblowing and electrospinning of fibrous diclofenac sodium-cyclodextrin complex-based reconstitution injection. J. Drug Deliv. Sci. Technol. 26, 28–34.

Bi, Y., Sunada, H., Yonezawa, Y., Danjo, K., Otsuka, A., IIDA, K., 1996. Preparation and evaluation of a compressed tablet rapidly disintegrating in the oral cavity. Chem. Pharm. Bull. 44, 2121–2127.

Bilensoy, E., 2011. Cyclodextrins in pharmaceutics, cosmetics, and biomedicine: current and future industrial applications. John Wiley & Sons.

Bukhary, H., Williams, G.R., Orlu, M., 2018. Electrospun fixed dose formulations of amlodipine besylate and valsartan. Int. J. Pharm. 549, 446–455.

Carneiro, S.B., Duarte, C., Ílary, F., Heimfarth, L., Quintans, S., de Souza, J., Quintans-Júnior, L.J., Veiga Júnior, V.F. da, Neves de Lima, Á.A., 2019. Cyclodextrin–Drug Inclusion Complexes: In Vivo and In Vitro Approaches. Int. J. Mol. Sci. 20, 642.

Celebioglu, A., Kayaci-Senirmak, F., İpek, S., Durgun, E., Uyar, T., 2016. Polymer-free nanofibers from vanillin/cyclodextrin inclusion complexes: high thermal stability, enhanced solubility and antioxidant property. Food Funct. 7, 3141–3153.

Celebioglu, A., Uyar, T., 2020. Hydrocortisone/cyclodextrin complex electrospun nanofibers for a fast-dissolving oral drug delivery system. RSC Med. Chem.

Celebioglu, A., Uyar, T., 2019a. Fast Dissolving Oral Drug Delivery System based on Electrospun Nanofibrous Webs of Cyclodextrin/Ibuprofen Inclusion Complex Nanofibers. Mol. Pharm.

Celebioglu, A., Uyar, T., 2019b. Metronidazole/Hydroxypropyl-β-Cyclodextrin Inclusion

Complex Nanofibrous Webs as Fast-dissolving Oral Drug Delivery System. Int. J. Pharm. 118828.

Celebioglu, A., Uyar, T., 2019c. Encapsulation and Stabilization of α-Lipoic Acid in Cyclodextrin Inclusion Complex Electrospun Nanofibers: Antioxidant and Fast-Dissolving α-Lipoic Acid/Cyclodextrin Nanofibrous Webs. J. Agric. Food Chem.

Ciper, M., Bodmeier, R., 2005. Preparation and characterization of novel fast disintegrating capsules (Fastcaps) for administration in the oral cavity. Int. J. Pharm. 303, 62–71.

Giram, P.S., Shitole, A., Nande, S.S., Sharma, N., Garnaik, B., 2018. Fast dissolving moxifloxacin hydrochloride antibiotic drug from electrospun Eudragit L-100 nonwoven nanofibrous Mats. Mater. Sci. Eng. C 92, 526–539.

Higuchi, T., Connors, K.A., 1965. Phase solubility diagram. Adv Anal Chem Instrum 4, 117–212.

Hsu, C.-M., Yu, S.-C., Tsai, F.-J., Tsai, Y., 2019. Characterization of in vitro and in vivo bioactivity of a ferulic acid-2-Hydroxypropyl-β-cyclodextrin inclusion complex. Colloids Surfaces B Biointerfaces 180, 68–74.

Huang, W., Yang, Y., Zhao, B., Liang, G., Liu, S., Liu, X.-L., Yu, D.-G., 2018. Fast dissolving of ferulic acid via electrospun ternary amorphous composites produced by a coaxial process. Pharmaceutics 10, 115.

Illangakoon, U.E., Gill, H., Shearman, G.C., Parhizkar, M., Mahalingam, S., Chatterton, N.P., Williams, G.R., 2014. Fast dissolving paracetamol/caffeine nanofibers prepared by electrospinning. Int. J. Pharm. 477, 369–379.

Juni Ekowati, N., Rahman, S.D., Dewi Isadiartuti, N., Widyowati, R.R., Budiati, T., 2016. Synthesis of Ferulic Acid and Its Non Covalent Inclusion with Hydroxypropyl-β-Cyclodextrin. Int. J. Pharm. Clin. Res. 8, 198–205.

Kalepu, S., Nekkanti, V., 2015. Insoluble drug delivery strategies: review of recent advances and business prospects. Acta Pharm. Sin. B 5, 442–453.

Kathpalia, H., Gupte, A., 2013. An Introduction to Fast Dissolving Oral Thin Film Drug Delivery Systems: A Review. Curr. Drug Deliv. https://doi.org/10.2174/15672018100613112515024 9

Kazsoki, A., Szabó, P., Domján, A., Balázs, A., Bozó, T., Kellermayer, M., Farkas, A., Balogh-Weiser, D., Pinke, B., Darcsi, A., 2018. Microstructural distinction of electrospun nanofibrous drug delivery systems formulated with different excipients. Mol. Pharm. 15, 4214–4225.

Kumar, N., Goel, N., 2019. Phenolic acids: Natural versatile molecules with promising therapeutic applications. Biotechnol. Reports e00370.

Kwak, H.W., Woo, H., Kim, I.-C., Lee, K.H., 2017. Fish gelatin nanofibers prevent drug crystallization and enable ultrafast delivery. RSC Adv. 7, 40411–40417.

Li, X., Kanjwal, M.A., Lin, L., Chronakis, I.S., 2013. Electrospun polyvinyl-alcohol nanofibers

as oral fast-dissolving delivery system of caffeine and riboflavin. Colloids Surfaces B Biointerfaces 103, 182–188.

Loftsson, T., Frikdriksdóttir, H., Sigurkdardóttir, A.M., Ueda, H., 1994. The effect of water-soluble polymers on drug-cyclodextrin complexation. Int. J. Pharm. 110, 169–177.

Loftsson, T., Hreinsdóttir, D., Másson, M., 2005. Evaluation of cyclodextrin solubilization of drugs. Int. J. Pharm. 302, 18–28.

Mancuso, C., Santangelo, R., 2014. Ferulic acid: pharmacological and toxicological aspects. Food Chem. Toxicol. 65, 185–195.

Mano, F., Martins, M., Sá-Nogueira, I., Barreiros, S., Borges, J.P., Reis, R.L., Duarte, A.R.C., Paiva, A., 2017. Production of electrospun fast-dissolving drug delivery systems with therapeutic eutectic systems encapsulated in gelatin. AAPS PharmSciTech 18, 2579–2585.

Mori, T., Tsuchiya, R., Doi, M., Nagatani, N., Tanaka, T., 2019. Solubilization of ultraviolet absorbers by cyclodextrin and their potential application in cosmetics. J. Incl. Phenom. Macrocycl. Chem. 93, 91–96.

Mura, P., 2015. Analytical techniques for characterization of cyclodextrin complexes in the solid state: A review. J. Pharm. Biomed. Anal. 113, 226–238.

Nagy, Z.K., Balogh, A., Démuth, B., Pataki, H., Vigh, T., Szabó, B., Molnár, K., Schmidt, B.T., Horák, P., Marosi, G., 2015. High speed electrospinning for scaled-up production of amorphous solid dispersion of itraconazole. Int. J. Pharm. 480, 137–142.

Nam, S., Lee, S.Y., Cho, H.-J., 2017. Phloretin-loaded fast dissolving nanofibers for the locoregional therapy of oral squamous cell carcinoma. J. Colloid Interface Sci. 508, 112–120.

Narayanan, G., Boy, R., Gupta, B.S., Tonelli, A.E., 2017. Analytical techniques for characterizing cyclodextrins and their inclusion complexes with large and small molecular weight guest molecules. Polym. Test. 62, 402–439.

Olga, G., Styliani, C., Ioannis, R.G., 2015. Coencapsulation of ferulic and gallic acid in hp-b-cyclodextrin. Food Chem. 185, 33–40.

Patel, V.F., Liu, F., Brown, M.B., 2011. Advances in oral transmucosal drug delivery. J. Control. release 153, 106–116.

Patil, P.C., Shrivastava, S.K., Vaidehi, S., Ashwini, P., 2014. Oral fast dissolving drug delivery system: a modern approach for patient compliance. Int. J. Drug Regul. Aff. 2, 49–60.

Peppas, N.A., Narasimhan, B., 2014. Mathematical models in drug delivery: How modeling has shaped the way we design new drug delivery systems. J. Control. Release 190, 75–81.

Poornima, B., Korrapati, P.S., 2017. Fabrication of chitosan-polycaprolactone composite nanofibrous scaffold for simultaneous delivery of ferulic acid and resveratrol. Carbohydr. Polym. 157, 1741–1749.

Qin, Z., Jia, X.-W., Liu, Q., Kong, B., Wang, H., 2019. Fast dissolving oral films for drug delivery prepared from chitosan/pullulan electrospinning nanofibers. Int. J. Biol. Macromol.

137, 224–231.

Quan, J., Yu, Y., Branford-White, C., Williams, G.R., Yu, D.-G., Nie, W., Zhu, L.-M., 2011. Preparation of ultrafine fast-dissolving feruloyl-oleyl-glycerol-loaded polyvinylpyrrolidone fiber mats via electrospinning. Colloids Surfaces B Biointerfaces 88, 304–309.

Rahane, R.D., Rachh, P.R., 2018. A review on fast dissolving tablet. J. Drug Deliv. Ther. 8, 50–55.

Rezaei, A., Varshosaz, J., Fesharaki, M., Farhang, A., Jafari, S.M., 2019. Improving the solubility and in vitro cytotoxicity (anticancer activity) of ferulic acid by loading it into cyclodextrin nanosponges. Int. J. Nanomedicine 14, 4589.

Samprasit, W., Akkaramongkolporn, P., Ngawhirunpat, T., Rojanarata, T., Kaomongkolgit, R., Opanasopit, P., 2015. Fast releasing oral electrospun PVP/CD nanofiber mats of taste-masked meloxicam. Int. J. Pharm. 487, 213–222.

Saokham, P., Muankaew, C., Jansook, P., Loftsson, T., 2018. Solubility of cyclodextrins and drug/cyclodextrin complexes. Molecules 23, 1161.

Seif, S., Franzen, L., Windbergs, M., 2015. Overcoming drug crystallization in electrospun fibers–Elucidating key parameters and developing strategies for drug delivery. Int. J. Pharm. 478, 390–397.

Sharif, N., Golmakani, M.-T., Niakousari, M., Hosseini, S., Ghorani, B., Lopez-Rubio, A., 2018. Active Food Packaging Coatings Based on Hybrid Electrospun Gliadin Nanofibers Containing Ferulic Acid/Hydroxypropyl-Beta-Cyclodextrin Inclusion Complexes. Nanomaterials 8, 919.

Sipos, E., Kósa, N., Kazsoki, A., Szabó, Z.-I., Zelkó, R., 2019. Formulation and characterization of aceclofenac-loaded nanofiber based orally dissolving webs. Pharmaceutics 11, 417.

Thakkar, S., More, N., Sharma, D., Kapusetti, G., Kalia, K., Misra, M., 2019. Fast dissolving electrospun polymeric films of anti-diabetic drug repaglinide: formulation and evaluation. Drug Dev. Ind. Pharm. 45, 1921–1930.

Topuz, F., Uyar, T., 2019. Electrospinning of Cyclodextrin Functional Nanofibers for Drug Delivery Applications. Pharmaceutics 11, 6.

Tort, S., Yıldız, A., Tuğcu-Demiröz, F., Akca, G., Kuzukıran, Ö., Acartürk, F., 2019. Development and characterization of rapid dissolving ornidazole loaded PVP electrospun fibers. Pharm. Dev. Technol. 24, 864–873.

Uyar, T., Besenbacher, F., 2008. Electrospinning of uniform polystyrene fibers: The effect of solvent conductivity. Polymer (Guildf). 49, 5336–5343.

Uyar, T., Kny, E., 2017. Electrospun materials for tissue engineering and biomedical applications: research, design and commercialization. Woodhead Publishing.

Vass, P., Démuth, B., Farkas, A., Hirsch, E., Szabó, E., Nagy, B., Andersen, S.K., Vigh, T., Verreck, G., Csontos, I., 2019. Continuous alternative to freeze drying: Manufacturing of cyclodextrin-based reconstitution powder from aqueous solution using scaled-up

electrospinning. J. Control. Release 298, 120–127.

Wang, H., Zhang, Y., Xia, T., Wei, W., Chen, F., Guo, X., Li, X., 2013. Synergistic promotion of blood vessel regeneration by astragaloside IV and ferulic acid from electrospun fibrous mats. Mol. Pharm. 10, 2394–2403.

Wang, J., Cao, Y., Sun, B., Wang, C., 2011. Characterisation of inclusion complex of trans-ferulic acid and hydroxypropyl-β-cyclodextrin. Food Chem. 124, 1069–1075.

Wang, Q., Yu, D.-G., Zhang, L.-L., Liu, X.-K., Deng, Y.-C., Zhao, M., 2017. Electrospun hypromellose-based hydrophilic composites for rapid dissolution of poorly water-soluble drug. Carbohydr. Polym. 174, 617–625.

Xu, M.-R., Shi, M., Bremner, D.H., Sun, K., Nie, H.-L., Quan, J., Zhu, L.-M., 2015. Facile fabrication of P (OVNG-co-NVCL) thermoresponsive double-hydrophilic glycopolymer nanofibers for sustained drug release. Colloids Surfaces B Biointerfaces 135, 209–216.

Xue, J., Wu, T., Dai, Y., Xia, Y., 2019. Electrospinning and electrospun nanofibers: Methods, materials, and applications. Chem. Rev. 119, 5298–5415.

Yakub, G., Ignatova, M., Manolova, N., Rashkov, I., Toshkova, R., Georgieva, A., Markova, N., 2018. Chitosan/ferulic acid-coated poly (ε-caprolactone) electrospun materials with antioxidant, antibacterial and antitumor properties. Int. J. Biol. Macromol. 107, 689–702.

Yan, J., White, K., Yu, D.-G., Zhao, X.-Y., 2014. Sustained-release multiple-component cellulose acetate nanofibers fabricated using a modified coaxial electrospinning process. J. Mater. Sci. 49, 538–547.

Yang, G.-Z., Li, J.-J., Yu, D.-G., He, M.-F., Yang, J.-H., Williams, G.R., 2017. Nanosized sustained-release drug depots fabricated using modified tri-axial electrospinning. Acta Biomater. 53, 233–241.

Yildiz, Z.I., Celebioglu, A., Uyar, T., 2017. Polymer-free electrospun nanofibers from sulfobutyl ether7-beta-cyclodextrin (SBE7-β-CD) inclusion complex with sulfisoxazole: Fast-dissolving and enhanced water-solubility of sulfisoxazole. Int. J. Pharm. 531, 550–558.

Yıldız, Z.I., Uyar, T., 2019. Fast-dissolving electrospun nanofibrous films of paracetamol/cyclodextrin-inclusion complexes. Appl. Surf. Sci.

Yu, D.-G., Li, J.-J., Williams, G.R., Zhao, M., 2018. Electrospun amorphous solid dispersions of poorly water-soluble drugs: A review. J. Control. release.

Yuan, C., Liu, B., Liu, H., 2015. Characterization of hydroxypropyl-β-cyclodextrins with different substitution patterns via FTIR, GC–MS, and TG–DTA. Carbohydr. Polym. 118, 36–40.

Zhang, M., Li, J., Jia, W., Chao, J., Zhang, L., 2009. Theoretical and experimental study of the inclusion complexes of ferulic acid with cyclodextrins. Supramol. Chem. 21, 597–602.

Zhao, Z., Moghadasian, M.H., 2008. Chemistry, natural sources, dietary intake and pharmacokinetic properties of ferulic acid: A review. Food Chem. 109, 691–702.

Figure Captions

Fig. 1. The chemical structure of (a) HP-β-CD and HP-γ-CD, and (b) ferulic acid. (c) The schematic representation of inclusion complex formation between ferulic acid and CD molecules, (d) and the electrospinning of ferulic acid/CD-IC NM.

Fig. 2. Phase solubility diagram of ferulic acid/HP-β-CD and ferulic acid/HP-γ-CD systems.

Fig. 3. (i) The photos of the solutions and (ii) the nanofibrous mats; (iii) SEM images and the fiber diameter distribution graphs of (a) HP-β-CD NM, (b) ferulic acid/HP-β-CD-IC NM, (c) HP-γ-CD NM and (d) ferulic acid/HP-γ-CD-IC NM.

Fig. 4. ^{1}H-NMR spectra of ferulic acid, ferulic acid/HP-β-CD-IC NM and ferulic acid/HP-γ-CD-IC NM. The samples were dissolved in *d6*-DMSO in order to record the ^{1}H-NMR spectra.

Fig. 5. The full and expanded range FTIR spectra of ferulic acid, HP-β-CD NM, ferulic acid/HP-β-CD-IC NM, HP-γ-CD NM, ferulic acid/HP-γ-CD-IC NM.

Fig. 6. (a) XRD patterns and (b) DSC thermograms of ferulic acid, HP-β-CD NM, ferulic acid/HP-β-CD-IC NM, HP-γ-CD NM, ferulic acid/HP-γ-CD-IC NM.

Fig. 7. TGA thermograms and derivatives of (a) ferulic acid, HP-β-CD NM, ferulic acid/HP-β-CD-IC NM and (b) ferulic acid, HP-γ-CD NM, ferulic acid/HP-γ-CD-IC NM.

Fig. 8. Time dependent release profiles of ferulic acid, ferulic acid/HP-β-CD-IC NM and ferulic acid/HP-γ-CD-IC NM.

Fig. 9. The disintegration behaviour of (a) HP-β-CD NM, (b) ferulic acid/HP-β-CD-IC NM, (c) HP-γ-CD NM, (d) ferulic acid/HP-γ-CD-IC NM.

CRediT authorship contribution statement

Asli Celebioglu: Conseptualization, Methodology, Validation, Investigation, Writing- Original draft preparation, Writing - Review & Editing

Tamer Uyar: Supervision, Resources, Conseptualization, Methodology, Project administration, Funding acquisition.

Declaration of interests

☒ The authors declare that they have no known competing financial interests or personal relationships that could have appeared to influence the work reported in this paper.

☐The authors declare the following financial interests/personal relationships which may be considered as potential competing interests:

Figure

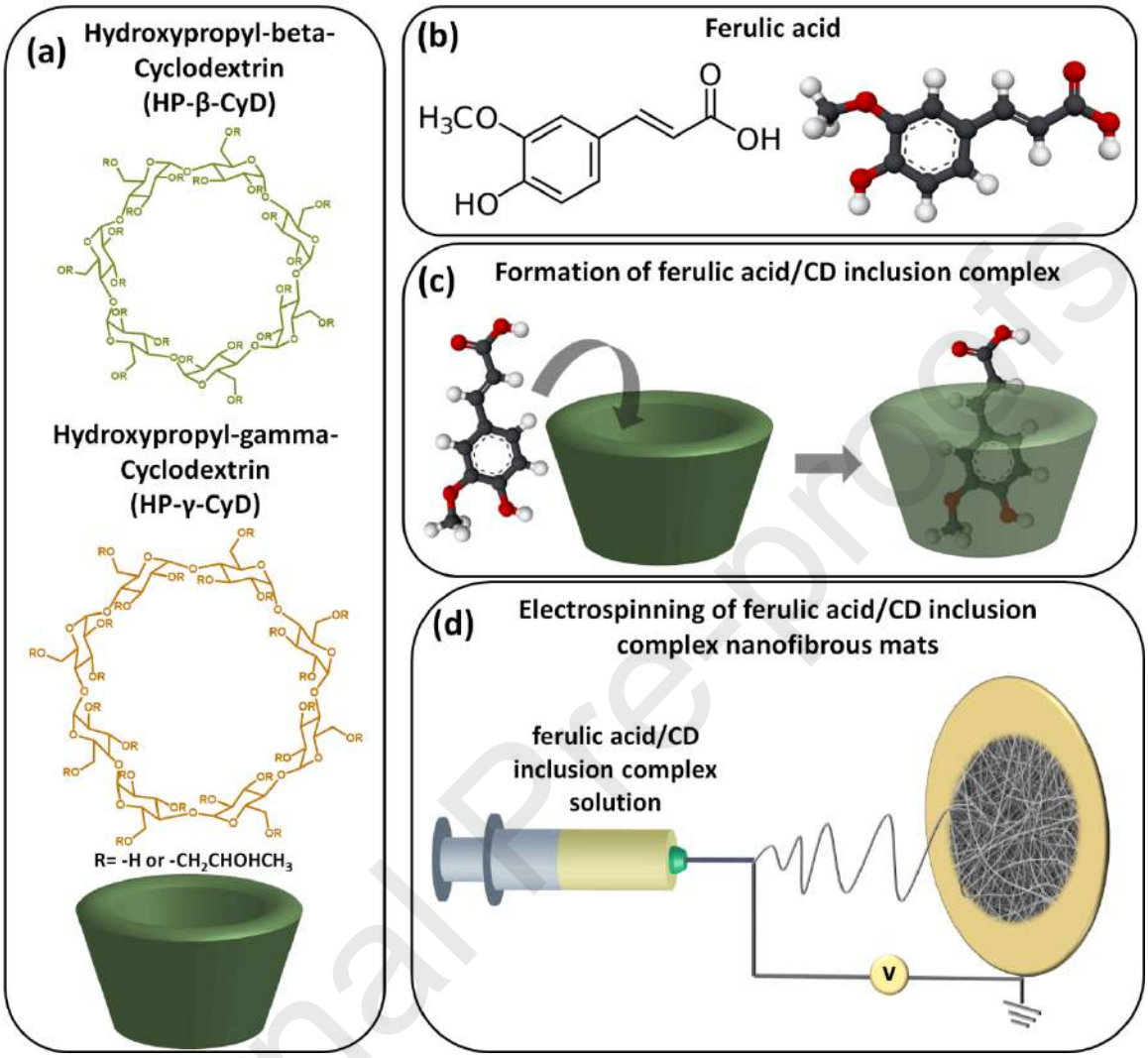

Fig. 1.

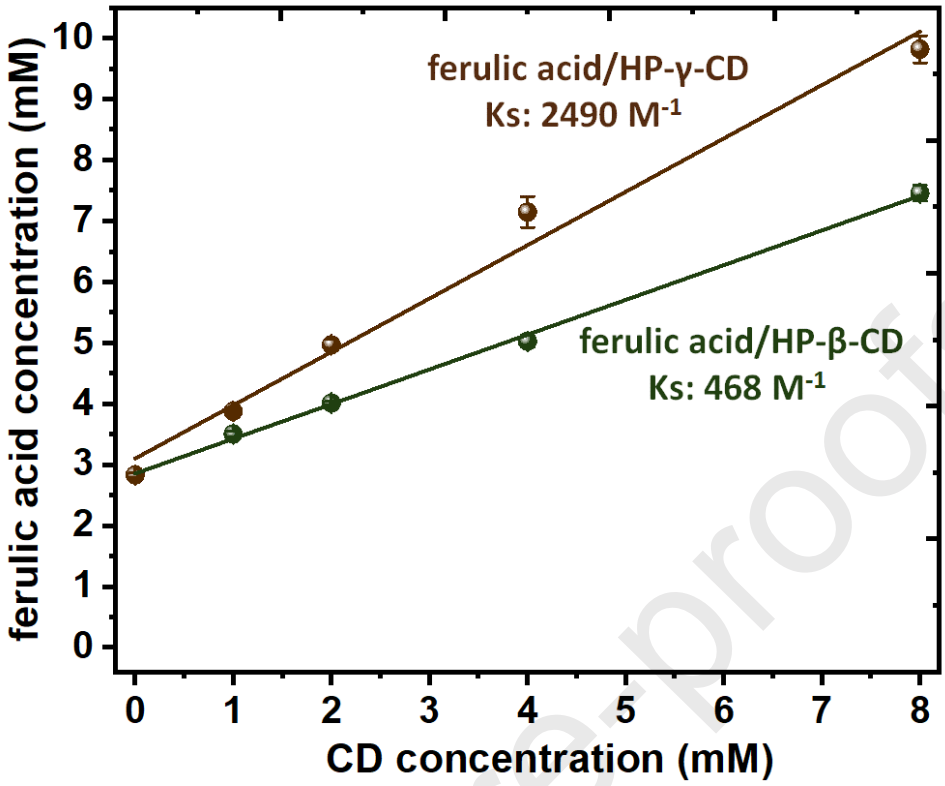

Fig. 2.

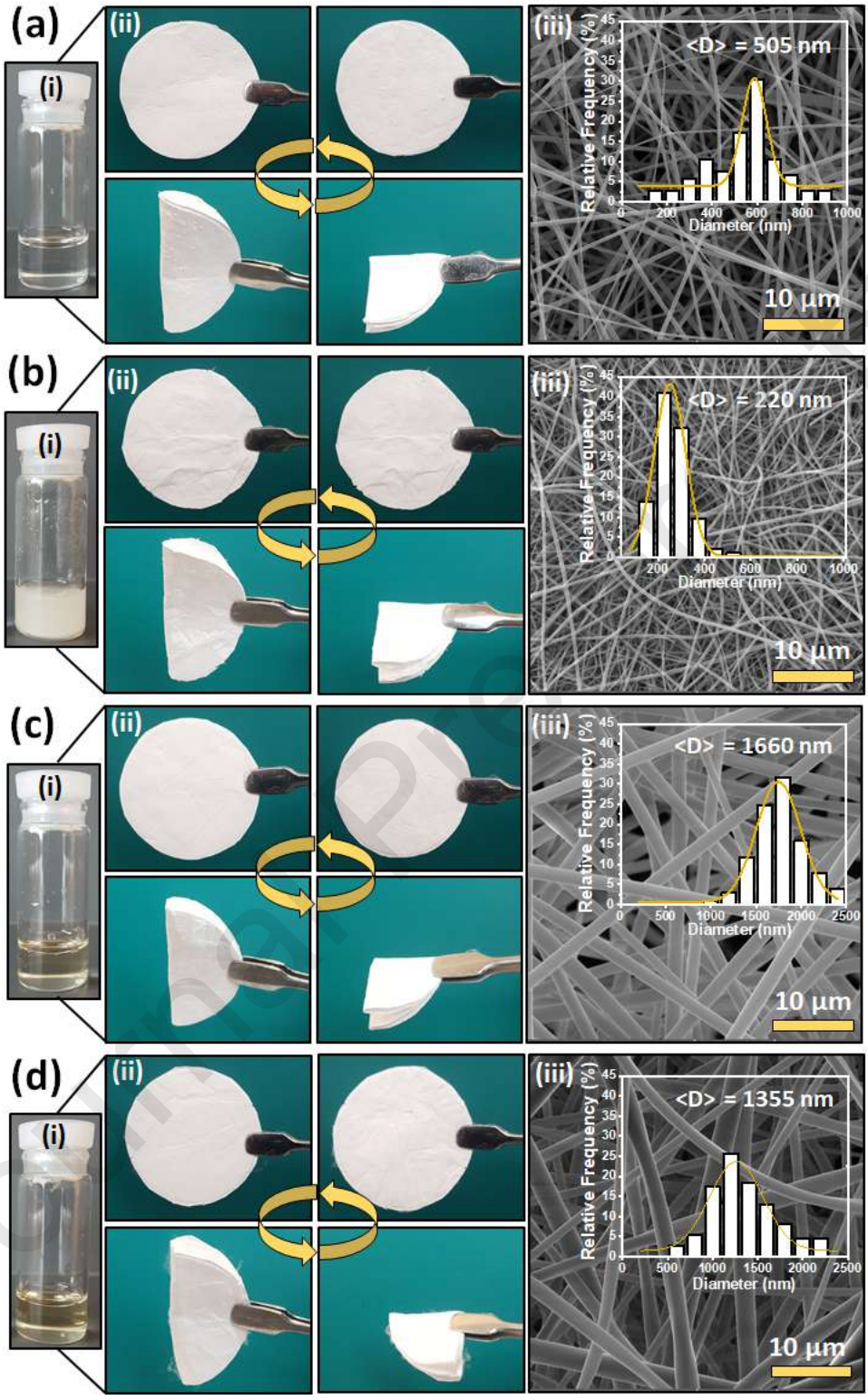
(a)
(i)
(ii)
(iii)
<D> = 505 nm
Relative Frequency (%)
Diameter (nm)
10 µm
(b)
(i)
(ii)
(iii)
<D> = 220 nm
Relative Frequency (%)
Diameter (nm)
10 µm
(c)
(i)
(ii)
(iii)
<D> = 1660 nm
Relative Frequency (%)
Diameter (nm)
10 µm
(d)
(i)
(ii)
(iii)
<D> = 1355 nm
Relative Frequency (%)
Diameter (nm)
10 µm

Fig. 3.

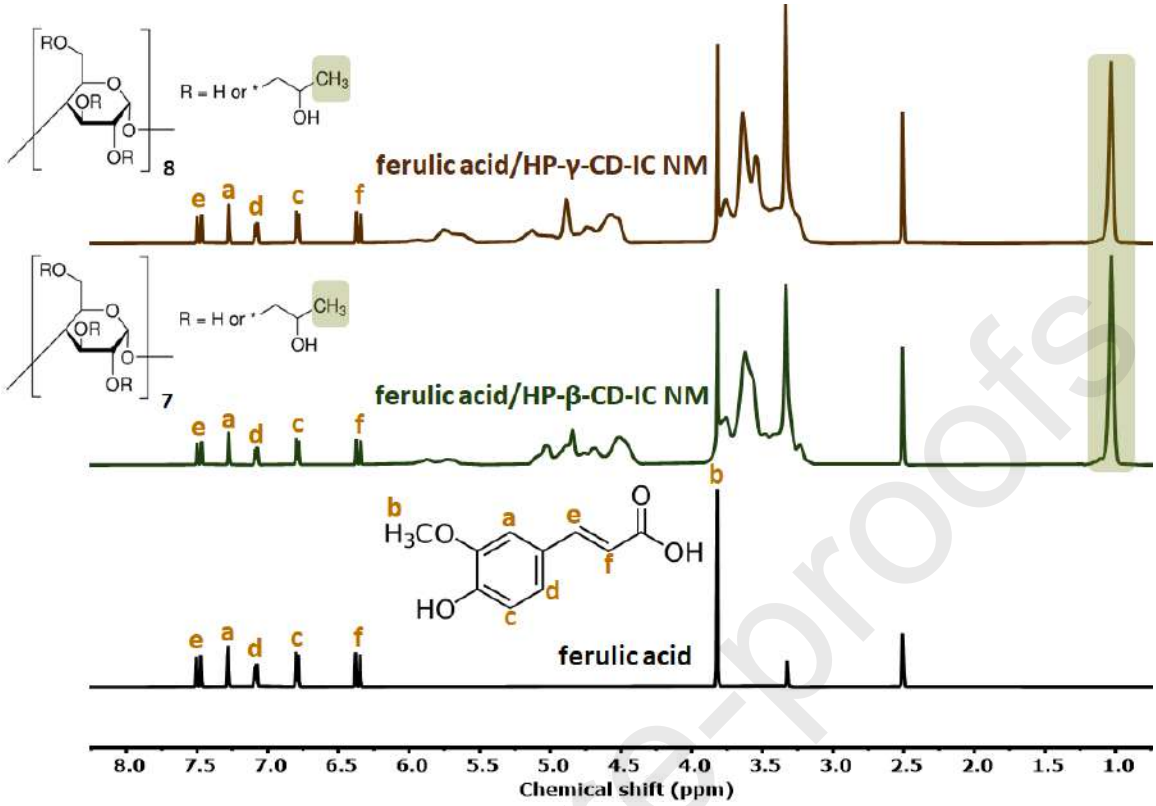

Fig. 4.

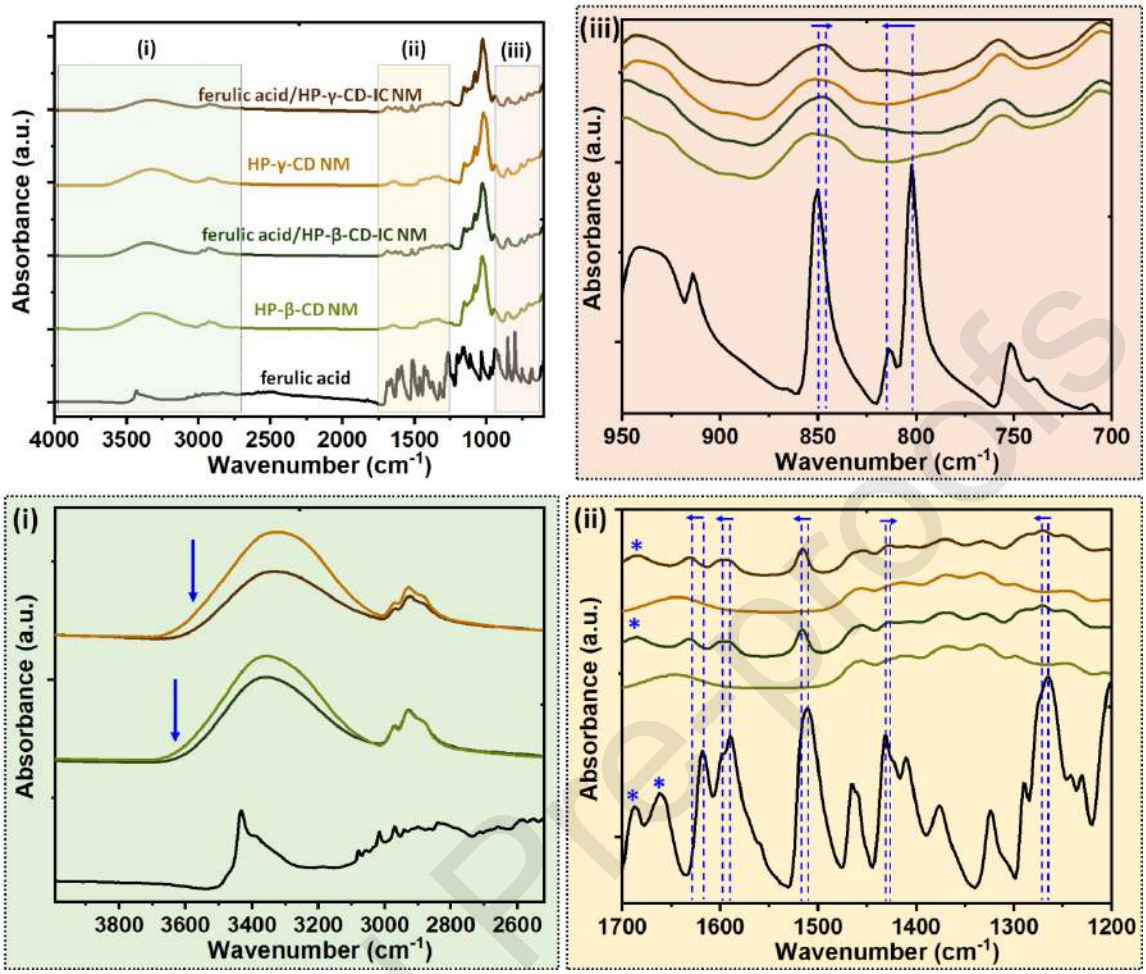

Fig. 5.

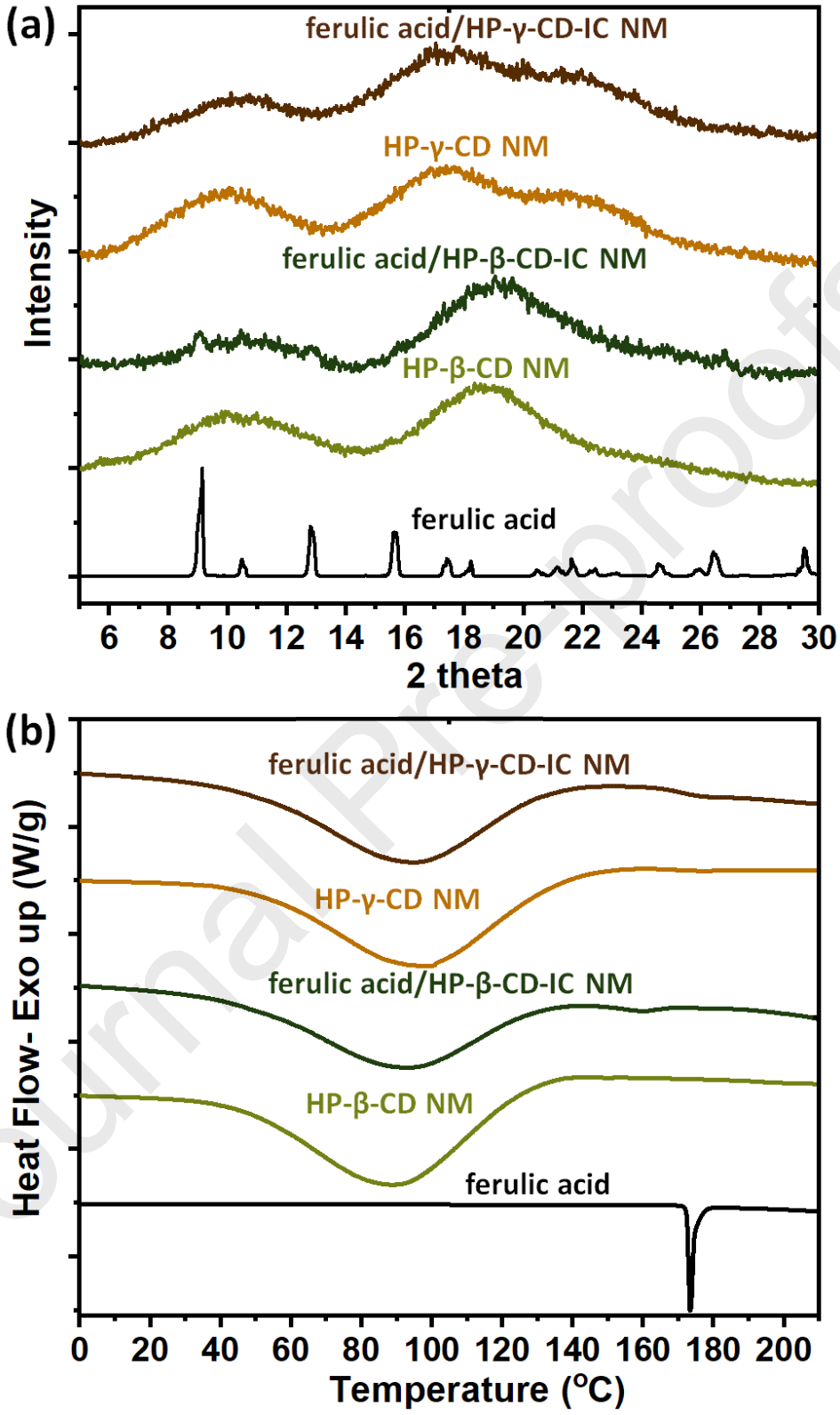
(a)
ferulic acid/HP-γ-CD-IC NM
HP-γ-CD NM
ferulic acid/HP-β-CD-IC NM
HP-β-CD NM
ferulic acid
Intensity
6 8 10 12 14 16 18 20 22 24 26 28 30
2 theta
(b)
ferulic acid/HP-γ-CD-IC NM
HP-γ-CD NM
ferulic acid/HP-β-CD-IC NM
HP-β-CD NM
ferulic acid
Heat Flow- Exo up (W/g)
0 20 40 60 80 100 120 140 160 180 200
Temperature (°C)

Fig. 6.

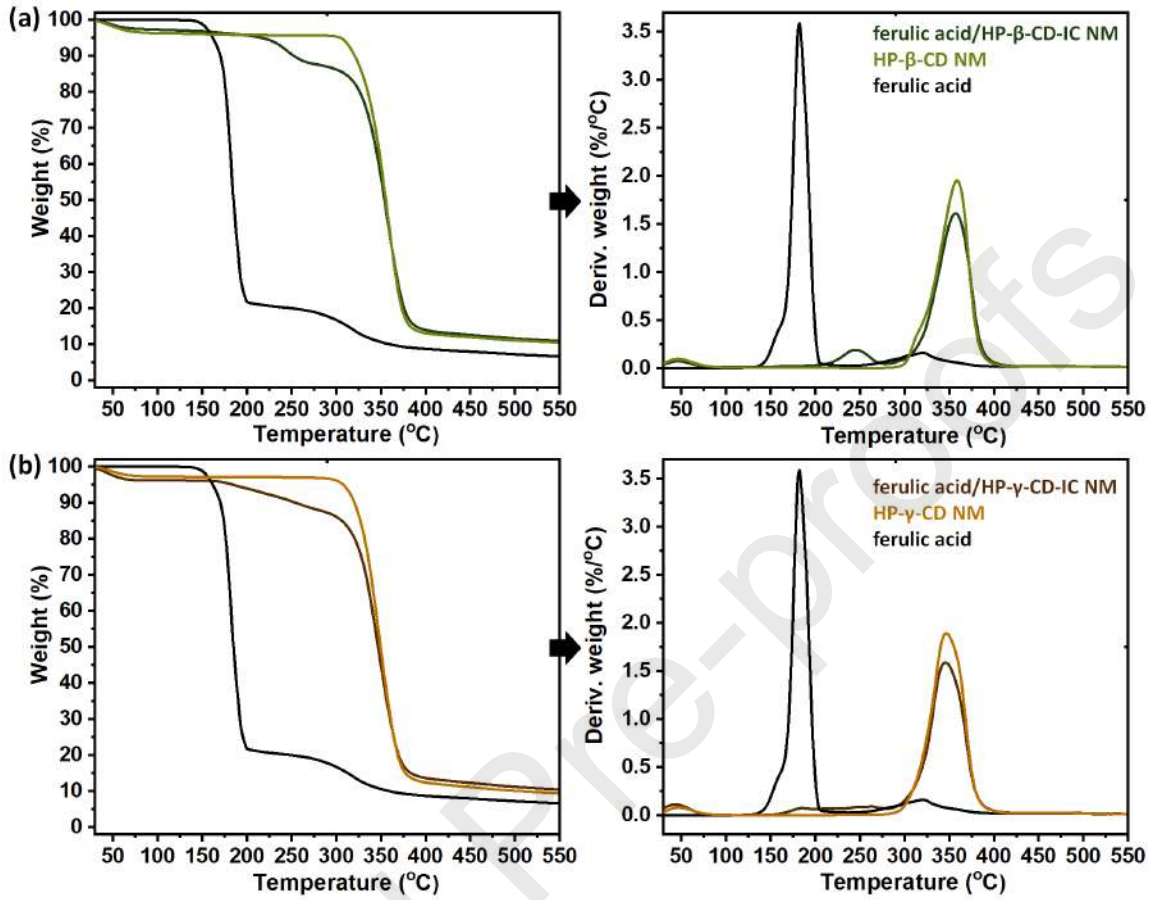

Fig. 7.

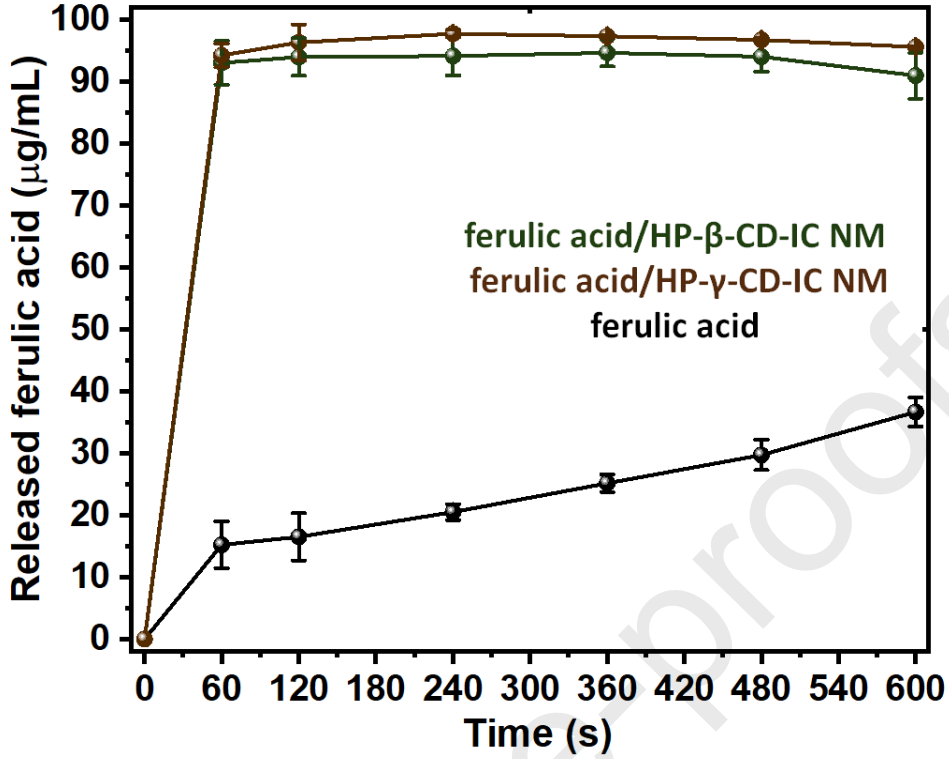

Fig. 8.

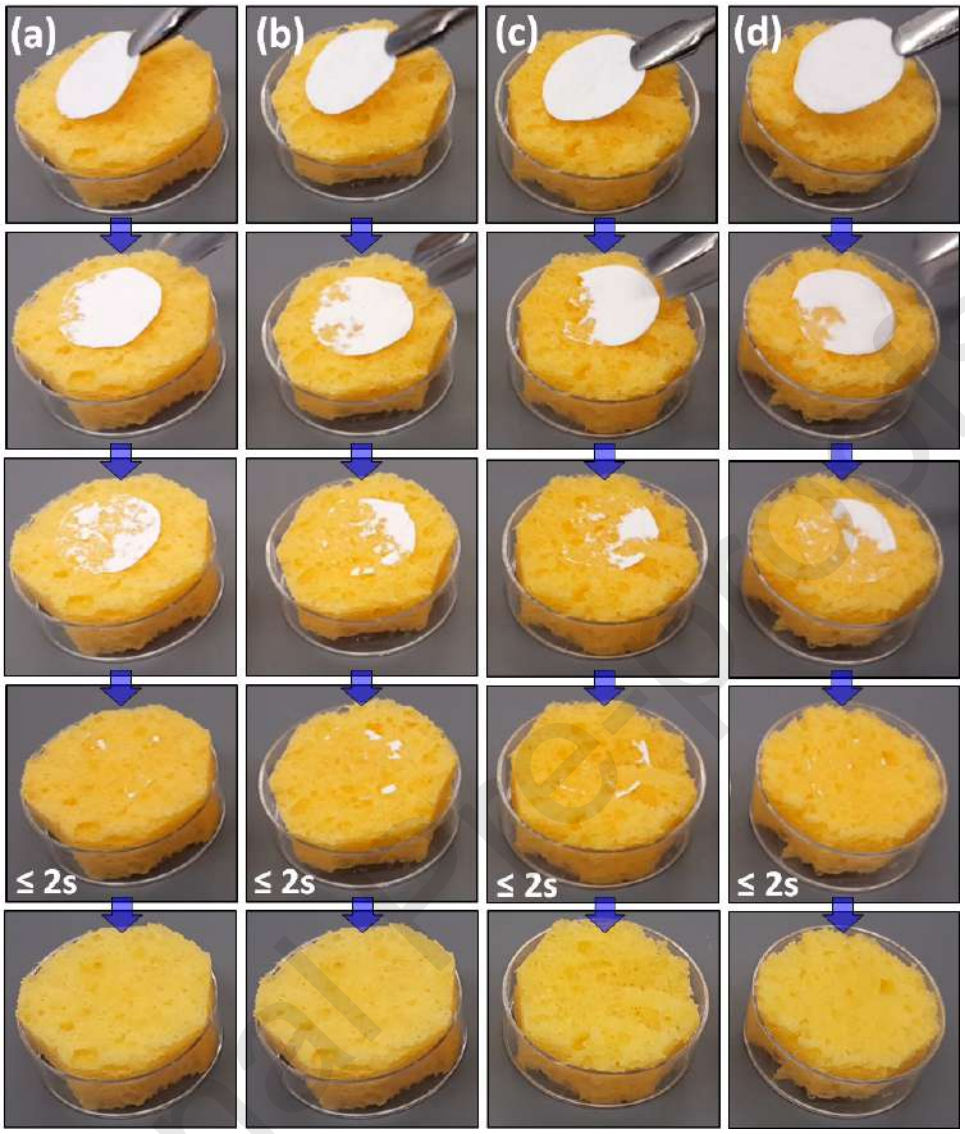

Fig. 9.

Table 1. The solution properties of viscosity and conductivity and the fiber diameters of resulting electrospun nanofibers.

Sample	Molar ratio (ferulic acid/CD)	CD concentration (%, w/v)	Viscosity (Pa·s)	Conductivity (μS/cm)	Average diameter (nm)
HP-β-CD	-	200	1.968	34.44	505±160
ferulic acid/ HP-β-CD	1/1	180	1.256	53.6	220±70
HP-γ-CD	-	200	2.661	6.10	1660±275
ferulic acid/ HP-γ-CD	1/1	180	1.585	11.4	1355±505